Hybrid mode-locking in a 40 GHz monolithic quantum dot laser

G. Fiol,[1,a)] D. Arsenijević,[1] D. Bimberg,[1] A. G. Vladimirov,[2,3] M. Wolfrum,[2] E. A. Viktorov,[4] and Paul Mandel[4]
[1]*Institut für Festkörperphysik, Technische Universität Berlin, Hardenbergstr. 36, 10623 Berlin, Germany*
[2]*Weierstrass Institute for Applied Analysis and Stochastics, Mohrenstrasse 39, D—10117 Berlin, Germany*
[3]*Physics Faculty, St. Petersburg State University, Ulianovskaya 3, 198504 St. Petersburg, Russia*
[4]*Optique Nonlinéaire Théorique, Université Libre de Bruxelles, Campus Plaine CP 231, B-1050 Bruxelles, Belgium*

(Received 19 October 2009; accepted 30 November 2009; published online 5 January 2010)

Hybrid mode-locking in monolithic quantum dot (QD) lasers is studied experimentally and theoretically. A strong asymmetry of the locking range with respect to the passive mode locking frequency is observed. The width of this range increases linearly with the modulation amplitude for all operating parameters. Maximum locking range found is 30 MHz. The results of a numerical analysis performed using a set of delay-differential equations taking into account carrier exchange between QDs and wetting layer are in agreement with experiments and indicate that a spectral filtering element could improve locking characteristics. © *2010 American Institute of Physics*. [doi:10.1063/1.3279136]

Quantum dot (QD) mode-locked lasers are promising for telecom applications since they demonstrate a number of important advantages as compared to standard quantum well (QW) devices.[1–3] However, tailoring the characteristics of QD lasers for specific applications is a challenging issue. An important characteristics of hybrid mode-locking (ML), a commonly used technique for improving quality of mode-locked pulses, is the frequency locking range where the pulse repetition frequency can be synchronized to that of the external signal. Since the first reports on 10 GHz hybrid ML (Ref. 4) a significant reduction of the pulse jitter has been demonstrated using hybrid ML with promising results of 124 and 190 fs for 40 GHz mode-locked lasers.[5,6] However, the so far achieved locking range for hybrid ML in QD lasers is smaller than that reported for QW devices. This fact was recently discussed in Ref. 7.

In this letter we study, experimentally and theoretically, the characteristics of the hybrid mode-locked regime in QD lasers with a pulse repetition rate of 40 GHz. We find that stable hybrid ML in QD lasers shows a locking range up to a few tens of MHz demonstrating a strong asymmetry with respect to the frequency of the free running passively mode-locked laser. We also discuss a possible improvement of hybrid ML locking range, and describe bifurcation mechanisms responsible for locking and unlocking between the fundamental ML regime and the external RF modulation.

Experimental investigations have been performed using a monolithic 40 GHz QD laser integrated in a module, comprising a standard single mode fiber pigtail and a microwave port. It is based on a two-section QD laser diode with a total length of 1 mm (saturable absorber length is 1/10 of the total length) and a 4 μm wide ridge waveguide structure. The active zone of the device contains 15 layers of self-organized InAs QDs emitting at 1.3 μm embedded in InGaAs quantum wells.[6] The threshold current density of the diode is 360 A/cm^2.

In the absence of the external modulation, the laser exhibits passive ML, which remains stable in a wide range of operating parameters. External modulation of the voltage V is applied to the absorber section of the device and has the form of $\bar{V}[1+a\cos(\Omega t)]$ where a, Ω, and $\bar{V}$ are the amplitude, frequency, and dc component of the reverse bias, respectively.

In order to investigate the locking range, the optical output of the laser diode was measured using a high speed 55 GHz bandwidth photodetector and a 50 GHz electrical spectrum analyzer. For various operating parameters (injection current in the gain section, reverse bias applied to the absorber section) the external frequency was varied around the cavity round trip frequency and from that the locking range was determined. The criterion to consider operation as locked to the external modulation was that the side band suppression ratio in the electrical spectra was larger than 30 dB. The transition from locked to unlocked state is rather sharp within our measurement resolution. Maximum locking range of ~30 MHz was achieved for the smallest values of current and reverse bias, requiring maximum modulation amplitude. For a fixed set of injection current and absorber bias (80 mA, −8 V) the variation of the modulation amplitude results in a locking tongue shown in Fig. 1, starting with about 7 MHz for the maximum applied modulation down to a sub MHz range for 0.4 Vpp (voltage peak-to-peak) or less. Linking the experimental modulation amplitude of 3.2 Vpp to the modulation amplitude a cannot be done with certainty, due to the fact that the absorber section is an unmatched load and external modulation power is partially reflected from it. In Fig. 1 3.2 Vpp can correspond to a value of modulation amplitude a between 0.4 and 0.8.

The locking range is strongly red-shifted and asymmetric with respect to the pulse repetition frequency of the passively mode-locked laser, as shown in the inset. The inset in Fig. 1 demonstrates the improvement of the jitter in hybrid operation by reduction of the linewidth, while pulsewidth and pulse shape stay the same, determined by autocorrelator measurements. The asymmetry is maintained for all amplitudes of the external signal. As discussed later, this asymme-

a)Electronic mail: gerrit.fiol@physik.tu-berlin.de.

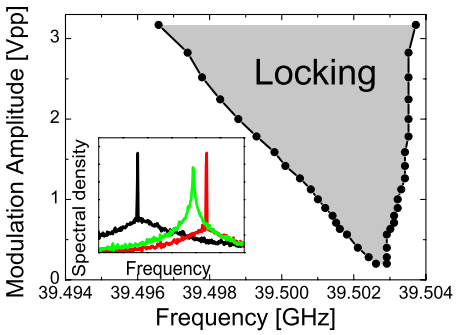

FIG. 1. (Color online) Experimentally measured change of the locking range for a fixed injection current and absorber bias with varying modulation amplitude (locking tongue). The dots are marking the borders of the locking range. The inset shows the asymmetry of the locking range (black and red line) with respect to the passive mode locking frequency (green line) for the maximum modulation amplitude of 3.2 Vpp.

try is related to the nonlinear frequency dependence of the amplitude of the locked solution. An extension of the measurement, where the injection current was kept fixed and the reverse bias is varied, is plotted in Fig. 2. Here only the overall locking range is evaluated. The values show a purely linear dependence on the modulation amplitude for all operating parameters. First, from −4 to −8 V the locking range decreases with bias. By increasing the bias further to −10 V the locking range gets larger again. This can be explained by comparing the behavior of the locking range to the optical pulse width, which has been obtained by measuring and fitting the autocorrelations. As it is shown in the inset of Fig. 2, shorter pulses with larger peak power exhibit smaller locking ranges.

To explain these observations, we use the model of a QD mode-locked laser described in Refs. 8 and 9. This model is described by a set of five delay differential equations

$$\gamma^{-1}\partial_t A(t) + A(t) = \sqrt{\kappa} e^{(1-i\alpha_g)G(t-T)/2+(1-i\alpha_q)Q(t-T)/2} A(t-T), \tag{1}$$

$$\partial_t \rho_g = N_g(1-\rho_g)/\tau_g^{\mathrm{cap}} - \rho_g/\tau_g^{\mathrm{esc}} - \rho_g/\tau_g - s_g I_g, \tag{2}$$

$$\partial_t N_g = (N_{g0}-N_g)/\tau_N - 2N_g(1-\rho_g)/\tau_g^{\mathrm{cap}} + 2\rho_g/\tau_g^{\mathrm{esc}}, \tag{3}$$

$$\partial_t \rho_{\mathrm{gs}} = 2\rho_{\mathrm{es}}(1-\rho_{\mathrm{gs}})/\tau_q^{\mathrm{cap}} - 2\rho_{\mathrm{gs}}(1-\rho_{\mathrm{es}})/\tau_q^{\mathrm{esc}} - \rho_{\mathrm{gs}}/\tau_q - s_q I_q, \tag{4}$$

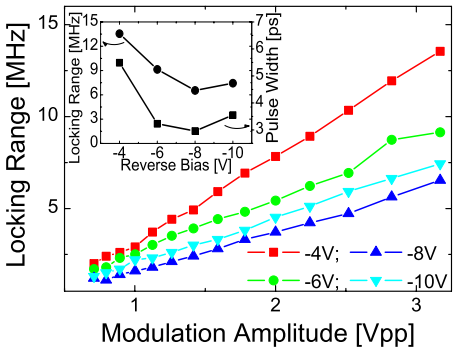

FIG. 2. (Color online) Dependence of measured locking range on the modulation amplitude. For a fixed gain current of 60 mA the absorber bias is varied in four steps while the locking range is measured in dependence of the modulation amplitude. The inset shows the behavior of the maximum locking range in comparison to the width of the optical pulses. The values for the locking range in the inset are for the highest modulation amplitude.

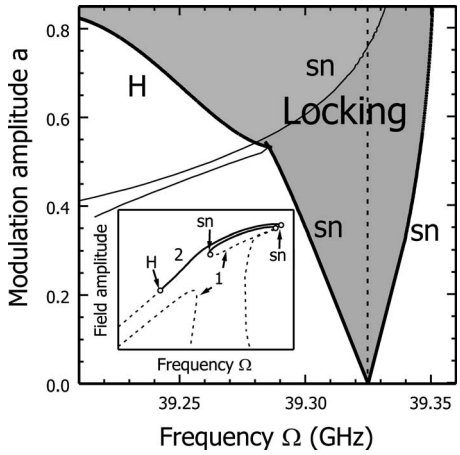

FIG. 3. Locking tongue calculated numerically. Thick lines indicate the stability boundaries of the locking regime (locking range). *sn*—saddle-node bifurcation lines. *H*—Andronov–Hopf bifurcation line. Thin lines correspond to saddle-node bifurcations of unstable solutions. Vertical dotted line is the passive mode-locked laser frequency. The inset shows branches of locked solutions. Stable (unstable) solutions are shown by solid (dotted) lines. (No. 1 is for $a=0.5$ and No. 2 for $a=0.7$). Empty dots indicate Hopf (h) and saddle-node (sn) bifurcations responsible for the destabilization of the locked solutions.

$$\partial_t \rho_{\mathrm{es}} = -\rho_{\mathrm{es}}/\tau_w - \rho_{\mathrm{es}}(1-\rho_q)\tau_q^{\mathrm{cap}} + \rho_{\mathrm{gs}}(1-\rho_{\mathrm{es}})/\tau_q^{\mathrm{esc}}, \tag{5}$$

where $A(t)$ is the normalized complex amplitude of the electric field at the entrance of the absorber section. $I_g = e^{-Q}(e^G-1)|A|^2$ and $I_q=(1-e^{-Q})|A|^2$.[8] The variables $G(t) = 2g_g L_g[2\rho_g(t)-1]$ and $Q(t)=2g_q L_q[2\rho_{\mathrm{gs}}(t)-1]$ are the time-dependent dimensionless cumulative saturable gain and absorption, and the parameters $g_{g,q}$ are the differential gains in the corresponding sections. The parameters $s_q > s_g$ are inversely proportional to the saturation intensities of the gain and absorber sections.

In Eqs. (1)–(5), the delay T is equal to the cold cavity round trip time. The attenuation factor $\kappa<1$ describes the total nonresonant linear intensity losses per cavity round trip. The dimensionless bandwidth of the spectral filtering is γ and the linewidth enhancement factor in the gain (absorber) section is $\alpha_g(\alpha_q)$.

The variables $\rho_g(t)$ and $N_g(t)$ are the dot occupation probability and the normalized carrier density in the wetting layer of the gain section. τ_g and τ_N are the recombination rates in the wetting layer and in the dots, respectively. The dimensionless parameter N_{g0} is a measure of carrier injection in the amplifier section. For this section, we use a carrier capture time of $\tau_g^{\mathrm{cap}}=10$ ps and an escape time $\tau_g^{\mathrm{esc}}=80$ ps.[10]

The carrier exchange dynamics for the absorber section is described by the occupation probabilities ρ_{gs} and ρ_{es} of the ground (GS) and the first excited (ES) state of a dot, respectively.[11,12] The parameters τ_q^{cap}, τ_q^{esc}, and τ_w determine the time-dependent recovery of the QD absorber. $\tau_q^{\mathrm{cap}}=2$ ps and $\tau_q^{\mathrm{esc}}=10$ ps, $\tau_w=\tau_{w0}\exp(|V(t)/V_0|)$, where $\tau_{w0}=18$ ps and $V_0\approx -2$ V. The modulation of the applied voltage results in $V(t)=\bar{V}[1+a\cos(\Omega t)]$, where $\bar{V}$ is the dc component of the reverse bias applied to the absorber section. Other parameters are: $\gamma=20$, $s=s_q/s_g=20$.

The numerical bifurcation diagram in Fig. 3 shows the locking tongue in two-parameter-plane, rf modulation frequency Ω, and amplitude a. The vertical dotted line indicates the pulse repetition frequency of the free running passively

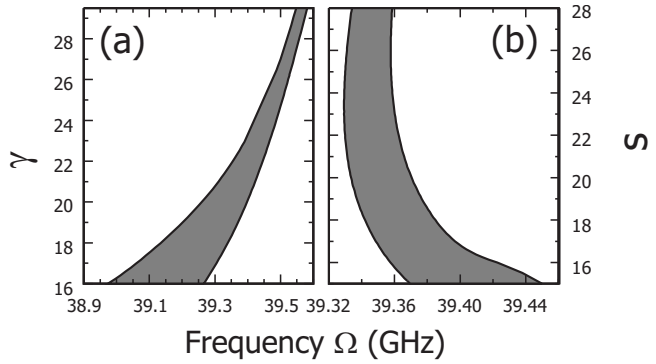

FIG. 4. Plots illustrating the dependence of the locking frequency range on the spectral filtering width γ (a) and ratio of the saturation intensities in gain and absorber sections $s=s_q/s_g$ (b). Locking domain is shown by gray color.

mode-locked laser ($a=0$). Figure 3 is very similar to the experimental results shown in Fig. 1. For sufficiently large modulation amplitudes the locking range is strongly asymmetric with respect to this frequency. The asymmetry is related to the nonlinear dependence of the pulse repetition frequency on the pulse amplitude, typical of nonlinear resonance phenomenon[13] (see inset in Fig. 3). The diagram in Fig. 3 demonstrates the fundamental difference between bifurcation mechanisms, leading to locking at small and large amplitude modulations. At small amplitudes of modulation ($a<0.52$) the locking domain has the form of a narrow tongue bounded by two saddle node bifurcation lines. This gives a sharp transition from locked to unlocked state in agreement with our experimental observations. In this case the branch of locked solutions is isolated in the parameter space, see inset of Fig. 3. When crossing the saddle-node line two locked solutions with periodic laser intensity, stable and unstable, merge and disappear, giving rise to a quasiperiodic motion on a torus. This is a standard mechanism of unlocking, typical for small amplitude modulation.

Another bifurcation mechanism of unlocking appears at sufficiently large modulation amplitudes a. The branch of locked solutions becomes connected to the unstable branch of modulated cw solutions, (see curve 2 in the inset of Fig. 3), the left saddle-node bifurcation line disappears in the cusp point, and the lower boundary of the locking range becomes limited by an Andronov–Hopf bifurcation. It is seen from the figure that this transition results in a significant increase of the locking range asymmetry. Similar transformations take place at the right boundary of the locking range. However, due to the strong asymmetry of the locking tongue, the Andronov–Hopf bifurcation at the right boundary of the locking tongue appears at larger modulation amplitudes than that at the left boundary (not shown in Fig. 3).

In agreement with the experimental data presented in the inset of Fig. 2, our simulations predict that shorter pulses with larger peak power have a smaller locking range. This is illustrated by Fig. 4(b), which shows the dependence of this range on the ratio $s=s_q/s_g$ of the saturation intensities in the gain and absorber sections. Increase of the parameter s leads usually to an increase of the ML stability domain and improvement of the pulse quality.[7,14,15] A similar decrease of the locking range is observed with the increase of the spectral filtering width γ which also leads to a decrease of the pulse width, see Fig. 4(a). This figure also explains the discrepancy between the values of the locking range widths shown in Figs. 1 and 3. For convenience in numerical simulations we have used rather small values of the parameter γ. Indeed, for $\gamma^{-1}=0$ the derivative disappears from the field Eq. (1) which becomes a discrete map. All the periodic solutions of this map have a period equal to the delay time T. Hence, such solutions will never synchronize to the external modulation if the modulation period differs from T. Increasing the locking range with the decreasing γ suggests that the inclusion of an additional spectral filtering section into the laser cavity can lead to an increase of the locking range [See Fig. 4(a)]. The experimentally determined optical spectra were three to four times wider than those calculated theoretically. This suggests that the value of γ approximating most closely the value of gain bandwidth is three to four times larger than that used in simulations.

In conclusion, we studied hybrid ML in a two section QD laser. The experiments demonstrate and the theory confirms, that the hybrid ML operation in QD lasers exhibits a strongly asymmetric locking range which is smaller than that for QW lasers. Our model explains the appearance of a locked state as a result of saddle node and inverse Andronov–Hopf bifurcations. Our numerical results indicate that the locking range in hybrid mode-locked QD lasers might be improved by incorporating an additional spectral filtering section.

A.G.V is grateful to D. Rachinskii and D. Turaev for stimulating discussions. The authors in Brussels acknowledge support of the Fonds National de la Recherche Scientifique (Belgium). The authors at TU Berlin and WIAS would like to acknowledge the funding of this work by the Grant No. SFB787 of the DFG.

[1] D. Bimberg, M. Grundmann, and N. N. Ledentsov, *Quantum Dot Heterostructures* (Wiley, Chichester, England, 1999).
[2] D. Bimberg, J. Phys. D **38**, 2055 (2005).
[3] D. Bimberg, Electron. Lett. **44**, 168 (2008).
[4] M. Thompson, C. Marinelli, K. Tan, K. Williams, R. Penty, I. White, I. Kaiander, R. Sellin, D. Bimberg, D.-J. Kang, M. G. Blamire, F. Visinka, S. Jochum, and S. Hansmann, Electron. Lett. **39**, 1121 (2003).
[5] M. G. Thompson, D. Larsson, A. Rae, K. Yvind, R. V. Penty, I. H. White, J. Hvam, A. R. Kovsh, D. L. S.Mikhrin, and I. Krestnikov, Proceedings of the Eur. Conf. Opt. Commun. (ECOC), Cannes, France, 2006, paper We 4.6.3.
[6] M. Kuntz, G. Fiol, M. Laemmlin, C. Meuer, and D. Bimberg, Proc. IEEE **95**, 1767 (2007).
[7] M. G. Thompson, A. R. Rae, M. Xia, R. V. Penty, and I. H. White, IEEE J. Sel. Top. Quantum Electron. **15**, 661 (2009).
[8] A. G. Vladimirov and D. Turaev, Phys. Rev. A **72**, 033808 (2005).
[9] E. A. Viktorov, P. Mandel, A. G. Vladimirov, and U. Bandelow, Appl. Phys. Lett. **88**, 201102 (2006).
[10] T. Erneux, E. A. Viktorov, P. Mandel, T. Piwonski, G. Huyet, and J. Houlihan, Appl. Phys. Lett. **94**, 113501 (2009).
[11] T. Piwonski, J. Pulka, G. Madden, G. Huyet, J. Houlihan, E. A. Viktorov, T. Erneux, and P. Mandel, Appl. Phys. Lett. **94**, 123504 (2009).
[12] E. A. Viktorov, T. Erneux, P. Mandel, T. Piwonski, G. Madden, J. Pulka, G. Huyet, and J. Houlihan, Appl. Phys. Lett. **94**, 263502 (2009).
[13] A. H. Nayfeh and D. T. Mook, *Nonlinear Oscillations* (Wiley, New York, 1979).
[14] D. Rachinskii, A. G. Vladimirov, U. Bandelow, B. Hüttl, and R. Kaiser, J. Opt. Soc. Am. B **23**, 663 (2006).
[15] B. Hüttl, R. Kaiser, C. Kindel, S. Fidorra, W. Rehbein, H. Stolpe, G. Sahin, U. Bandelow, M. Radziunas, A. G. Vladimirov, and H. Heidrich, Appl. Phys. Lett. **88**, 221104 (2006).